Ultralow threshold on-chip microcavity nanocrystal quantum dot lasers

Bumki Min, Sungjee Kim, Koichi Okamoto, Lan Yang, Axel Scherer et al.

Citation: Appl. Phys. Lett. **89**, 191124 (2006); doi: 10.1063/1.2387966
View online: http://dx.doi.org/10.1063/1.2387966
View Table of Contents: http://apl.aip.org/resource/1/APPLAB/v89/i19
Published by the American Institute of Physics.

Additional information on Appl. Phys. Lett.

Journal Homepage: http://apl.aip.org/
Journal Information: http://apl.aip.org/about/about_the_journal
Top downloads: http://apl.aip.org/features/most_downloaded
Information for Authors: http://apl.aip.org/authors

ADVERTISEMENT

Downloaded 19 Apr 2013 to 143.248.118.122. This article is copyrighted as indicated in the abstract. Reuse of AIP content is subject to the terms at: http://apl.aip.org/about/rights_and_permissions

Ultralow threshold on-chip microcavity nanocrystal quantum dot lasers

Bumki Min and Sungjee Kim[a)]
Department of Applied Physics, California Institute of Technology, Pasadena, California 91125

Koichi Okamoto
Department of Physics, California Institute of Technology, Pasadena, California 91125

Lan Yang, Axel Scherer, Harry Atwater, and Kerry Vahala[b)]
Department of Applied Physics, California Institute of Technology, Pasadena, California 91125

(Received 6 July 2006; accepted 4 October 2006; published online 9 November 2006)

Chemically synthesized nanocrystal, CdSe/ZnS (core/shell), quantum dots are coated on the surface of an ultrahigh-Q toroidal microcavity and the lasing is observed at room and liquid nitrogen temperature by pulsed excitation of quantum dots, either through tapered fiber or free space. Use of a tapered fiber coupling substantially lowered the threshold energy when compared with the case of free space excitation. The reason for the threshold reduction is attributed to the efficient delivery of pump pulses to the active gain region of the toroidal microcavity. Further threshold reduction was possible by quantum dot surface-coverage control. By decreasing the quantum dot numbers on the surface of the cavity, the threshold energy is further decreased down to 9.9 fJ. © *2006 American Institute of Physics*. [DOI: 10.1063/1.2387966]

Reduction of laser threshold can be obtained by leveraging large oscillator strength gain media with modern, high-quality-factor (Q factor)/high-spatial-confinement resonator designs. Along these lines, two emerging strategies have been pursued as a means to explore the limits of classical laser performance. In the first, high-spatial-confinement (small mode volume) semiconductor microcavities offering moderate Q factors are loaded with epitaxially grown, self-assembled semiconductor quantum dots (QDs) with impressive results.[1] In the latter, whispering-gallery resonators providing high-Q performance with moderate spatial confinement have been coated/filled with strongly quantum confined, semiconductor colloidal dots to also achieve excellent performance.[2–4] As a chip-based microcavity providing Q factors in excess of 10^8, silica toroidal microcavity resonators provide both long photon storage times and improved spatial confinement over microsphere resonators of comparable size.[5] The devices are also fabricated at lithographically predefined locations on a silicon chip which provides additional benefits over microsphere resonators. Furthermore, with highly ideal, tapered-fiber coupling, efficient pumping and laser emission extraction are possible.[6]

Ultrahigh-Q silica toroidal microcavities and tapered-fiber waveguides are fabricated by the procedures published earlier.[5] The waist diameter of the tapered-fiber center can be adiabatically reduced down to around 1 μm allowing pump pulses to be coupled evanescently to the toroidal microcavity. CdSe/ZnS (core/shell) QDs of high photoluminescence quantum yield (>50%) are similarly synthesized as published previously[7] [Fig. 1(a)]. The QDs are dispersed in toluene and spin cast on toroidal microcavities. Typical QD thicknesses explored in this work were a few densely packed layers down to ~0.3% (submonolayer) surface coverage. Surface coverage was estimated from spectrophotometric measurements of the solutions that have retrieved QDs from the spun-cast wafer surfaces.[8] (There can be errors in counting the number of QDs on the active area of the toroidal microcavity. However, the order of magnitude estimation can be obtained with this method.) Figure 1(b) shows the schematic experimental setup. Figure 1(c) shows a scanning electron microscopy image of a representative QD cast toroidal microcavity with a minor/principal diameter of 5/60.6 μm. The lasing emission is bidirectionally coupled out of the cavity [Fig. 1(d)] and measured at one end of the tapered fiber either by a streak camera with a time resolution of 20 ps or by a liquid-nitrogen-cooled charge coupled device (CCD) spectrometer.

To understand the loading conditions affecting pump and signal coupling, we studied the effect of QD surface coverage on the total intrinsic Q factor of the toroidal microcavity. The intrinsic Q will be affected primarily by QD absorption at a particular wavelength as well as Rayleigh scattering caused by the discrete nature of the QDs as dielectric nanoparticles ($Q_0^{-1}=Q_{\mathrm{abs}}^{-1}+Q_{\mathrm{scatter}}^{-1}$). Figure 2 shows the theoretical intrinsic Q factors (based on measured absorption and scattering parameters) for two surface-coverage densities. The Q factor in the absence of QDs is assumed to be in excess of 10^8. (The adsorbed water molecules on the surface have a negligible effect on Q factor at the visible wavelength.[9]) At wavelengths well above the absorption band of the QDs, the Q factor is QD scattering limited as illustrated by $Q_{\mathrm{scatter}}^{-1} \propto \lambda^{-7/2}$. However, at the pump wavelength the Q factor is absorption limited and estimated to be in the range from 2×10^4 to 3×10^6 depending on the coverage density [$Q_{\mathrm{abs}}^{-1} \propto \lambda\sigma_{\mathrm{QD}}(\lambda)n_{\mathrm{QD}}\Gamma(\lambda)$, where $\sigma_{\mathrm{QD}}(\lambda)$, n_{QD}, and $\Gamma(\lambda)$ are QD absorption cross section,[8] QD concentration, and modal overlap factor calculated from the normalized QD concentration profile and mode intensity pattern of the toroidal microcavity, respectively]. The measured intrinsic Q factor at 682 nm is 1.2×10^7 for low coverage density (~0.3%) and is consistent with a scattering limited Q as inferred from the model.

Pulsed excitation is used for all experiments to avoid the Auger process that competes with stimulated emission[10] in the strongly confined regime. The pulse is frequency doubled to 388 nm from a mode-locked Ti:sapphire laser having a

[a)]Present address: Department of Chemistry, Pohang University of Science and Technology, San 31 Hyojadong, Pohang 790-784, Republic of Korea.
[b)]Electronic mail: vahala@caltech.edu; URL: http://vahala.caltech.edu

 © 2006 American Institute of Physics

Downloaded 19 Apr 2013 to 143.248.118.122. This article is copyrighted as indicated in the abstract. Reuse of AIP content is subject to the terms at: http://apl.aip.org/about/rights_and_permissions

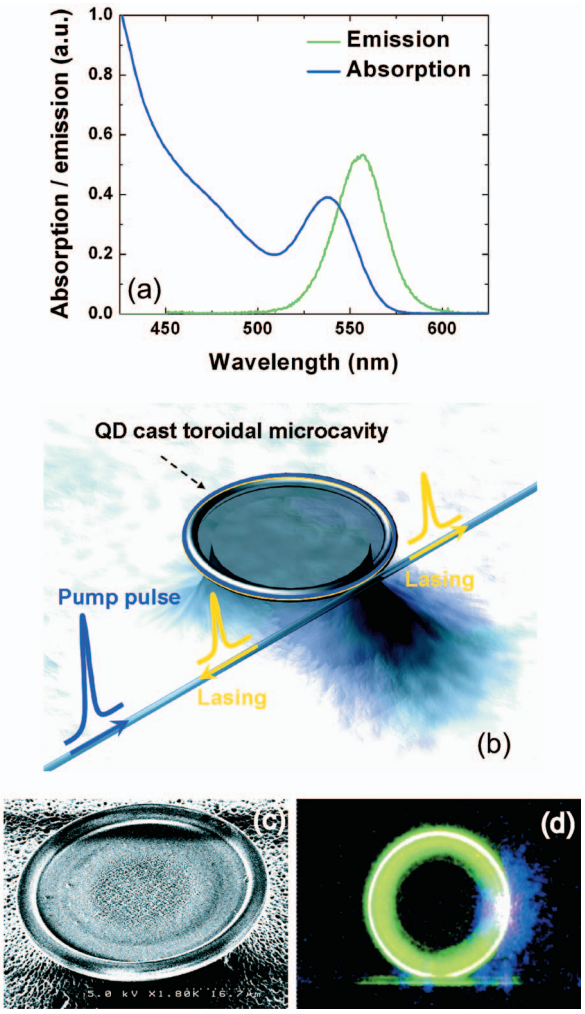

FIG. 1. (Color) (a) Absorption and photoluminescence spectra of QDs in hexane solution. The nanocrystal diameter is estimated to be ~2.6 nm. (b) Schematic experimental setup of a tapered-fiber-coupled, toroidal microcavity, nanocrystal QD laser. Pump pulses are coupled to the microcavity and lasing pulses are bidirectionally emitted through the tapered fiber. Pulse repetition rate is 80 MHz and pump wavelength is 388 nm. The output emission is collected either by a streak camera or by a high-resolution, liquid-nitrogen-cooled, CCD spectrometer. (c) Scanning electron micrograph of QD spin-cast toroidal microcavity. The principal diameter of the toroidal microcavity is ~60.6 μm. (d) Optical micrograph of a tapered-fiber-coupled, toroidal microcavity, nanocrystal QD laser showing QD emission from the whispering-gallery mode. Tapered fiber and toroidal microcavity are kept in contact during pumping.

pulse width of <100 fs and a repetition rate of 80 MHz. Optimal pump coupling resulted when tapered fiber and toroidal microcavity were in contact. This arrangement indicates the presence of strong pump-band absorption provided by the QDs. Based on measured pump coupling (10%–30%) and the estimated pump Q factor (see Fig. 2), the waveguide-resonator loading is in the undercoupled regime. Furthermore, the absorption-limited pump-band Q is so low so as to enable efficient coupling of even short pulses, which themselves are spectrally broad (for toroidal cavities used here, there exist many higher-order modes at the pump wavelength in addition to the fundamental pump mode and the presence of these modes with low Q factors can result in an improved coupling). Depending on the sample, both single mode and multi mode lasings have been observed. Representative single mode lasing is shown in Fig. 3(a) with the lasing peak at 579 nm. Figure 3(b) shows a multimode spectrum at

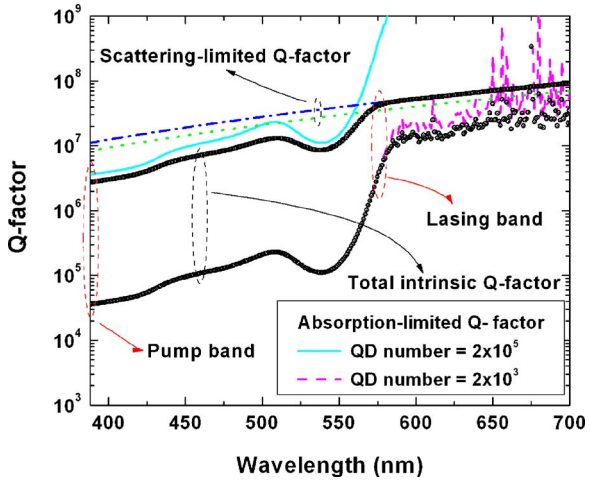

FIG. 2. Theoretical total intrinsic Q factors for two different surface coverages of QDs on a toroidal microcavity (circle/rectangle—high/low coverage). QD scattering-limited Q factors (dot/dash-dot—high/low coverage) and absorption-limited Q factors (solid/dash—high/low coverage) are also shown.

slightly higher pump excitation. The measured mode spacing of approximately 5 nm is larger than the next-nearest neighbor spacing (~1 nm) and is consistent with spectral hole burning in the gain distribution.[11] The lasing spectra are obtained by integrating 50 ps windows after each excitation pulse. To demonstrate the improved laser efficiency obtained by using a tapered-fiber coupling, free space excitation of the toroidal microcavity QD laser was conducted. Figure 4(a) shows typical data for the output emission power as a function of free space pump excitation energy (L-L curve) at 77 K and room temperature. It is worth noting that the threshold energies are not very sensitive to the temperature change. This is a characteristic of QDs in strong confinement regime and is in contrast to other epitaxially grown large QDs. For comparison to the free space pumping case, Fig. 4(b) shows an L-L curve measured using a tapered-fiber-coupled QD laser at room temperature with other conditions kept identical. A threshold energy (~1 pJ, in the left panel) is measured and represents a reduction by a factor of ~2600 when compared to the free space excitation case. This reduc-

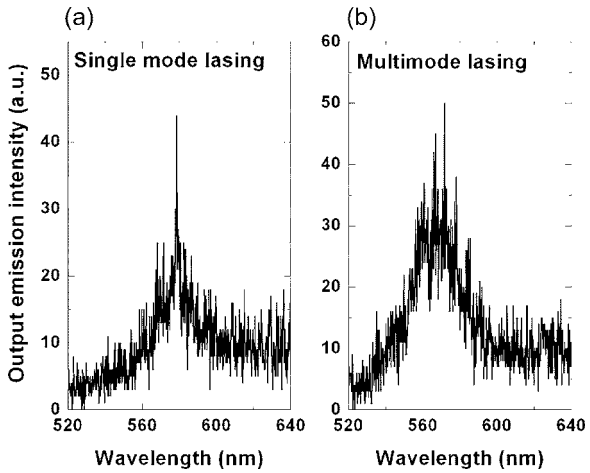

FIG. 3. Single mode and multimode lasing spectra from tapered-fiber-coupled toroidal microcavity QD lasers. Spectra are integrated over a time window of 50 ps after each pulse excitation. (a) Single mode lasing spectrum. (b) Multimode lasing spectrum.

Downloaded 19 Apr 2013 to 143.248.118.122. This article is copyrighted as indicated in the abstract. Reuse of AIP content is subject to the terms at: http://apl.aip.org/about/rights_and_permissions

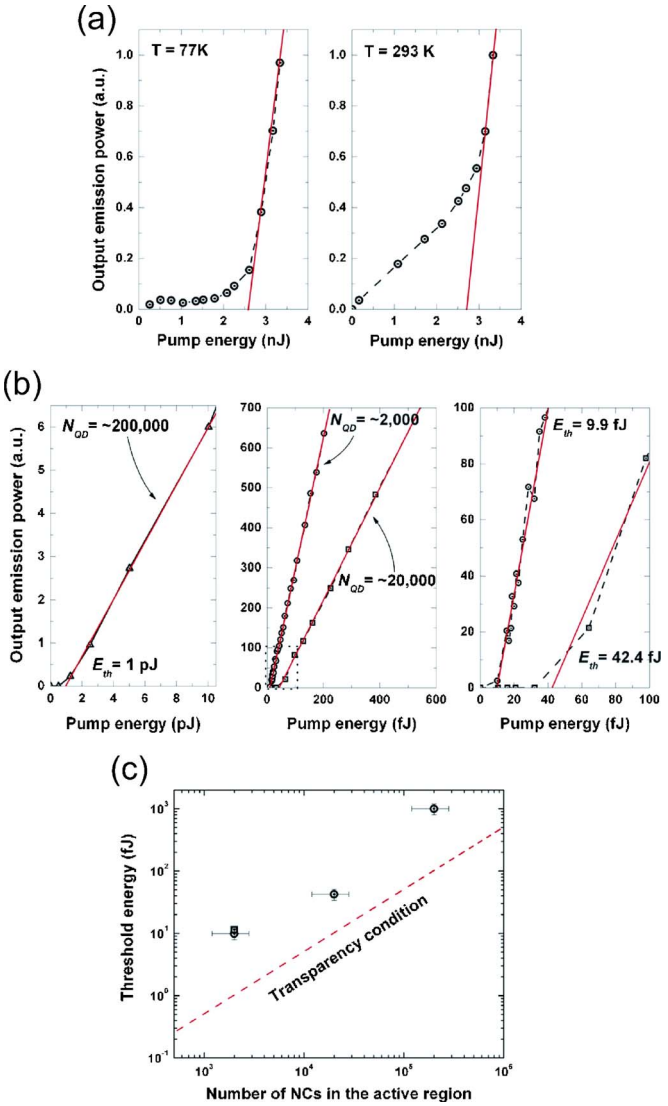

FIG. 4. *L-L* curves from toroidal microcavity nanocrystal QD lasers and threshold energies from tapered-fiber-coupled toroidal microcavity QD lasers with varying number of QDs in the active region (output emission powers for different concentration samples are not related to each other). (a) *L-L* curves from toroidal microcavity QD lasers excited via free space pumping. Two *L-L* curves are shown for two different temperatures (77 and 293 K). (b) *L-L* curves from toroidal microcavity QD lasers excited via tapered-fiber coupling. Output emission power plotted as a function of input pump energy at the tapered-fiber microcavity junction for three samples with different numbers of QDs in the active gain region. For a sample with ~2000 QDs in the active region, an ultralow threshold energy of 9.9 fJ is observed. For clarity, the *L-L* data curves are repeated (rightmost panel) with a magnified pump/emission scaling (corresponding to the boxed area in the center panel). (c) Plot of experimentally obtained threshold pump energies as a function of estimated number of nanocrystal quantum dots in the active region of the toroidal microcavity. The theoretical limit to pump energy provided by the transparency condition is denoted by a slanted line.

tion of threshold energy can be explained by the more efficient delivery of pump energy to the QD gain region as compared to the free space excitation case.

We next studied the effect of reducing the number of QDs on the threshold. By decreasing the number of QDs in the active gain region, two benefits can be obtained. First, the cavity *Q* factor is increased by reducing QD-related contribution to scattering/absorption loss (Fig. 2) and this in turn reduces the required optical gain to achieve threshold. Second, and most important, the transparency condition is lowered in proportion to the numeric reduction in QDs within the gain region. Concerning this latter effect, the threshold pump energy consists of both a transparency component and a "gain" component. Optimization of threshold therefore requires a balance of these two components that can be achieved experimentally through variation of the QD number. To test for an optimum threshold, two other samples having a decreased number of QDs [Fig. 4(b)] were measured. Threshold pump energies of 42.4 and 9.9 fJ are obtained for ~20000 and ~2000 QDs within the active region. In Fig. 4(c) the measured threshold pump energies are plotted as a function of the estimated number of QDs in the active region. For comparison, the theoretical lower bound on threshold energy provided by the transparency condition is also plotted. It is apparent that for decreasing QD number the measured threshold and lower bound begin to diverge. This can result from two mechanisms. First, as already noted, the gain component of pump energy will ultimately become a significant fraction of pump energy with decreasing QD number. Second, with decreasing QD number the pump-band *Q* factor will increase, thereby reducing the efficacy of pump coupling.

These observed improvements in laser threshold demonstrate the effectiveness of colloidal QDs as a tool to explore the limits of laser performance in the strongly confined regime, and, in addition, the utility of tapered fiber coupling. In addition, from a fundamental viewpoint, the measurement of 9.9 fJ is a record low threshold for strongly confined QDs and is close to the transparency bound for operation in this regime. Significantly, this result is obtained for room temperature operation, a result of using the strongly confined quantum dot lasing medium. More generally, the ability to coat microresonators on a chip with semiconductor nanocrystals can open up use of other nanocrystal surface functionalizations for operation in the visible/infrared or potentially for sensing applications.

This work was supported by the plasmonic MURI. Correspondence and requests for materials should be addressed to one of the authors (K.V.). Another author (B.M.) thanks Y.-B. Park for measuring AFM images of QD cast toroidal microcavity surfaces.

[1]S. Strauf, K. Hennessy, M. T. Rakher, Y.-S. Choi, A. Badolato, L. C. Andreani, E. L. Hu, P. M. Petroff, and D. Bouwmeester, Phys. Rev. Lett. **96**, 127404 (2006); K. Srinivasan, M. Borselli, T. J. Johnson, P. E. Barclay, O. Painter, A. Stintz, and S. Krishna, Appl. Phys. Lett. **86**, 151106 (2005).
[2]M. Kazes, D. Y. Lewis, Y. Ebenstein, T. Mokari, and U. Banin, Adv. Mater. (Weinheim, Ger.) **14**, 317 (2002).
[3]A. V. Malko, A. A. Mikhailovsky, M. A. Petruska, J. A. Hollingsworth, H. Htoon, M. G. Bawendi, and V. I. Klimov, Appl. Phys. Lett. **81**, 1303 (2002).
[4]P. T. Snee, Y. Chan, D. G. Nocera, and M. G. Bawendi, Adv. Mater. (Weinheim, Ger.) **17**, 1131 (2005).
[5]D. K. Armani, T. K. Kippenberg, S. M. Spillane, and K. J. Vahala, Nature (London) **421**, 925 (2003).
[6]M. Cai, O. Painter, and K. J. Vahala, Phys. Rev. Lett. **85**, 74 (2000).
[7]M. A. Hines and P. Guyot-Sionnest, J. Phys. Chem. **100**, 468 (1996).
[8]C. A. Leatherdale, W. K. Woo, F. V. Mikulec, and M. G. Bawendi, J. Phys. Chem. B **106**, 7619 (2002).
[9]D. W. Vernooy, V. S. Ilchenko, H. Mabuchi, E. W. Streed, and H. J. Kimble, Opt. Lett. **23**, 247 (1998).
[10]V. I. Klimov, A. A. Mikhailovsky, S. Xu, A. Malko, J. A. Hollingsworth, C. A. Leatherdale, H. Eisler, and M. G. Bawendi, Science **290**, 314 (2000).
[11]M. Shim and P. Guyot-Sionnest, Phys. Rev. B **64**, 245342 (2001).

Downloaded 19 Apr 2013 to 143.248.118.122. This article is copyrighted as indicated in the abstract. Reuse of AIP content is subject to the terms at: http://apl.aip.org/about/rights_and_permissions